AGU PUBLICATIONS

Water Resources Research

RESEARCH ARTICLE
10.1002/2014WR016724

Improved snow interception modeling using canopy parameters derived from airborne LiDAR data

D. Moeser[1,2], M. Stähli[3], and T. Jonas[1]

[1]WSL Institute for Snow and Avalanche Research SLF, Davos Dorf, Switzerland, [2]Forest Ecology, Institute of Terrestrial Ecosystems, Department of Environmental Sciences, Swiss Federal Institute of Technology ETH, Zurich, Switzerland, [3]Swiss Federal Institute for Forest, Snow and Landscape Research WSL, Birmensdorf, Switzerland

Key Points:
- Showed a 27% increase in r^2 and 40% RMSE reduction compared to prior models
- Canopy parameters that represent large-scale features explained most variations
- Nine thousand interception measurements indicated a sigmoidal shaped interception efficiency

Correspondence to:
D. Moeser,
moeser@slf.ch

Citation:
Moeser, D., M. Stähli, and T. Jonas (2015), Improved snow interception modeling using canopy parameters derived from airborne LiDAR data, *Water Resour. Res.*, *51*, 5041–5059, doi:10.1002/2014WR016724.

Received 26 NOV 2014
Accepted 4 JUN 2015
Accepted article online 6 JUN 2015
Published online 3 JUL 2015

Abstract Forest snow interception can account for large snow storage differences between open and forested areas. The effect of interception can also lead to significant variations in sublimation, with estimates varying from 5 to 60% of total snowfall. Most current interception models utilize canopy closure and LAI to partition interception from snowfall and calculate interception efficiency as an exponential decrease of interception efficiency with increasing precipitation. However, as demonstrated, these models can show specific deficiencies within heterogeneous canopy. Seven field areas were equipped with 1932 surveyed points within various canopy density regimes in three elevation bands surrounding Davos, Switzerland. Snow interception measurements were taken from 2012 to 2014 (~9000 samples) and compared with measurements at two open sites. The measured data indicated the presence of snow bridging from a demonstrated increase in interception efficiency as precipitation increased until a maximum was reached. As precipitation increased beyond this maximum, the data then exhibited a decrease in interception efficiency. Standard and novel canopy parameters were developed using aerial LiDAR data. These included estimates of LAI, canopy closure, distance to canopy, gap fraction, and various tree size parameters. These canopy metrics and the underlying efficiency distribution were then integrated to formulate a conceptual model based upon the snow interception measurements. This model gave a ~27% increase in the r^2 (from 0.39 to 0.66) and a ~40% reduction in RMSE (from 5.19 to 3.39) for both calibration and validation data sets when compared to previous models at the point scale. When upscaled to larger grid sizes, the model demonstrated further increases in performance.

1. Introduction

The hydrology of cold forested regions is dominated by snow forest processes and plays a significant role within the global water budget. Snowmelt dominated watersheds which contain forests yield approximately 60% of the global freshwater runoff [*Chang*, 2003]. Within the Northern hemisphere, it is estimated that 20% of the seasonal snow cover is located within forested areas and can account for 17% of total terrestrial water storage during the winter season [*Guntner et al*., 2007; *Rutter et al*., 2009].

In the Northern boreal forests, these processes are especially pronounced, with many internal forest snow mechanisms showing not just regional or local dependencies but demonstrating heterogeneity at extremely fine scales. Specifically, the surrounding forest structure can both augment and attenuate the physical forcing processes affiliated with snow accumulation and ablation. A prime example, intercepted snow from the forest canopy, ranges from 0 to just over 60% of total annual snowfall [*Montesi et al*., 2003; *Storck et al*., 2002]. Intercepted snow in most cases represents water lost, since this is the primary driver of sublimated snow in forested areas. Sublimation, like interception also demonstrates a significant range in values, and many studies have estimated sublimation to range up to 50% of the total annual snowfall [*Essery et al*., 2009; *Hedstrom and Pomeroy*, 1998; *Lundberg and Halldin*, 2001]. This large range of interception when paired with similarly large sublimation estimates makes interception the single most dominate physical process to drive snow cover heterogeneity in forest regions.

Snow interception has been studied for over 100 years, with the initial studies from *Carpenter* [1901] and *Church* [1912] which qualitatively describe forest snow interception. To date, three papers known to the authors have attempted to synthesize the results of these studies and highlight the contrasting methods

utilized to measure and represent interception processes [*Bunnell et al.,* 1985; *Lundberg and Halldin*, 2001; *Varhola et al*., 2010b]. If anything, these results serve to highlight the complexity of the phenomenon and emphasize that despite the large volumes of prior work; still more is needed to create an interception model valid over various conditions at various scales.

Many papers have highlighted the importance of snow bridging, branch bending, and snow bouncing on the maximum snow load and interception efficiency (interception/total precipitation) or the fraction of SWE which is intercepted in the canopy. *Tennyson et al.* [1974] and *Bründl* [1999] visually captured these processes using time lapse photography/video and showed an initial increase in snow interception efficiency on both Ponderosa pine and Norwegian spruce. The adhesion and cohesion processes leading toward snow bridging (potential surface area increase as well as potential broadening of the stress bulb) and the subsequent (initial) interception efficiency increase has been described qualitatively by *Bunnell et al*. [1985] and *Miller* [1964]. The first attempts to quantify these relationships were seen in the works of *Satterlund and Haupt* [1967] who developed a model in a Douglas fir and white pine forest which represented the underlying interception efficiency distribution as the growth phase of a sigmoidal curve. This work was furthered by *Schmidt and Gluns* [1991] who found a similar sigmoidal distribution in interception and efficiency in the branches of Engelmann spruce, subalpine fir, lodgepole pine, and artificial branches. However, the magnitude of the interception (and efficiency) was higher with the artificial branches implying interception depends on the bending potential of the branch or more specifically initial branch stiffness and the initial branch angle.

The model from *Hedstrom and Pomeroy* [1998] was one of the first to directly include canopy parameterizations (LAI and canopy closure (CC)). The model, based on their initial assumptions that interception efficiency (1) decreases with canopy snow load and (2) increases with canopy density, used an exponential decay model as the underlying efficiency distribution which contrasted to the majority of the prior findings.

Due to the inherent difficulties in direct interception measurements, a variety of inventive methods have been implemented in the past works. However, the standard direct method is destructive and necessitates the cutting of a tree which is then attached to a scale [*Hedstrom and Pomeroy*, 1998; *Nakai et al*., 1994, 1999; *Pomeroy et al*., 1998b; *Satterlund and Haupt*, 1967; *Schmidt and Gluns*, 1991; *Storck et al*., 2002; *Suzuki and Nakai*, 2008]. Optical methods have also been employed, which relate the visually intercepted snow load from time lapse photography to field measurements [*Brundl et al*., 1999; *Kobayashi*, 1987; *Nakai et al*., 1999; *Tennyson et al*., 1974]. Gamma Ray attenuation has also been used to directly measure the snow water equivalence on branches [*Calder*, 1991]. Due to the heavy material reliance of these direct methods, no data over larger scales has been collected. Of the above examples which also presented direct model equations for interception, the largest data set was collected by *Schmidt and Gluns* [1991] for a total of 175 branch samples (30–36 cm in length) over two seasons. *Satterlund and Haupt* [1967] used four tree saplings (3.7–4.2 m) for a one season study and *Hedstrom and Pomeroy* [1998] used four jack pine trees (7–15 m in height and 38–90 kg in weight) over four seasons and one black spruce tree (12 m in height and 22 kg in weight) over one season.

Like interception measurements, direct methods for measurement of canopy structure are also labor intensive and normally require destructive sampling of the overhead canopy. However, there are many indirect methods including hemispherical photography, plant canopy analyzers (LAI-2000), and spherical densitometers and each have particular strengths and weaknesses depending on the specific structure element estimated [*Breda*, 2003; *Hyer and Goetz*, 2004]. Airborne laser scanning (ALS) data are increasingly utilized to accurately estimate CC and LAI and are readily available for large areas throughout the world [*Lovell et al*., 2003; *Moeser et al*., 2014; *Morsdorf et al*., 2004, 2006; *Riaño et al*., 2004; *Solberg*, 2010; *Solberg et al*., 2009]. ALS can also derive large-scale features such as canopy openings within forested areas and it is also possible to provide information on how these open areas are positioned relative to the surrounding forest. Since ALS can quickly characterize surfaces over large scales, it can also be used for a variety of novel canopy parameter estimates potentially valuable for forest snow modeling. Investigations of large-scale canopy features represent a significant research gap with large potential improvements in a variety of research fields which has just begun to be investigated [*Moeser et al*., 2015; *Varhola et al*., 2010a; *Zhao et al*., 2011].

The Snow Model Inter-comparison Project (SnowMIP2) recognized 33 snow melt models which have directly integrated a snow interception module of varying degrees of complexity [*Essery et al*., 2009; *Rutter*

et al., 2009]. All of these models, utilize either canopy closure (CC), leaf area index (LAI), or a composite of the two in order to describe the canopy structure, with the majority directly utilizing the proposed algorithm by *Hedstrom and Pomeroy* [1998]. However, the interplay between generalized canopy characteristics such as LAI and CC and snow interception also depends on where these characteristics are situated in relation to surrounding forest architecture. As an example, field areas that have differing large-scale canopy structures such as forest gaps around a point can still have the same LAI or CC estimate.

Canopy gaps have large impacts on the snow holding capacity in many forested areas. These areas can show divergent snow accumulation patterns as compared to the surrounding forest and may have snow accumulation that exceeds nearby open, nonforested areas [*Troendle and Meiman*, 1986; *Winkler et al*., 2005]. The interface between the open and forested areas also show the most heterogeneous snow accumulation and ablation patterns within a forested area and can house both the maxima and minima depending upon the position relative to the surrounding forest [*Golding and Swanson*, 1986; *Veatch et al*., 2009]. In efforts to describe the relationship between openness and surrounding canopy, some practitioners categorize gaps for opening size as a function of the average surrounding tree size.

In order to permit for more robust interception modeling at landscape scales, the greater canopy topography as well as the spatial heterogeneity of canopy structure needs to be accounted for within models. Despite this, interception modules continue to use only point-based predictors, most likely due to the intensive requisite time involved in collecting canopy parameters over large areas. The inclusion of parameters which describe point-based canopy topography (canopy closure) with those which give information regarding where these parameters reside in relation to larger encompassing features such as the distribution of gaps around a point (e.g., total open area around a point), could allow for better upscaling of snow forest models to the landscape scale [*Moeser et al*., 2015]. ALS (when compared to manual collection methods) has the ability to provide such parameters over large scales, in a time and cost effective manner.

In order to develop a model that includes the greater canopy structure and allow for greater transferability of results, interception measurements are also needed over a large distribution of heterogeneous canopy architectures. With some assumptions, storm interception can be indirectly measured by comparing the ratio of newly fallen snow in the open to the amount newly fallen snow under the canopy. Typically this is done by measuring the new snow accumulation on top of preplaced boards [*Kobayashi*, 1987; *Lundberg et al*., 1998; *Pfister and Schneebeli*, 1999].

This research has utilized a novel indirect snow interception measurement method at thousands of surveyed measurements points (1932) within various canopy density and openness regimes over a series of interception events for a total of 9000 manually measured snow interception points (A) (cf. 4–175 samples from past studies). These interception estimates were then paired with novel canopy parameterizations from ALS data (B) in order to create a new interception model. This model integrated prior interception efficiency distribution research performed from branch, sapling, and tree studies and scaled these to be effectively used over forest landscape scales from the integration of novel canopy parameters from ALS data.

This is the first study to utilize such a large database of interception measurements (A) as well as use novel canopy parameters which integrate larger scale canopy structure (B) for an interception model. We have highlighted the (1) basic process flow of this pairing and (2) demonstrated the utility by a comparison to the most used snow interception model to date [*Hedstrom and Pomeroy*, 1998] under a broad range of canopy conditions and scales.

Furthermore, the *Hedstrom and Pomeroy* model, of which we compared our model skill, was created in a cold boreal climate but is often utilized in a variety of different meteorological environments. This should emphasize the need for not just a model integrating larger scale canopy structure, but one better suited for temperate snow environments.

2. Methods

2.1. Field Areas

Seven 50 m × 50 m forested field areas have been equipped for study in three unique elevation bands. They were set up in the fall of 2012 and are part of a long-term forest snow hydrology study area operated

by the WSL Institute for Snow and Avalanche Research (SLF). The field areas were characterized by highly heterogeneous canopy characteristics at the subplot scale along with the presence of larger scale canopy attributes such as canopy gaps. The field areas were further chosen to have low to no surface slopes and minimal surrounding terrain shading influences. The canopy was composed of predominately Norwegian spruce with heights varying from seedling to a maximum of 45 m, with the majority between 10 and 30 m. Each field area contained 276 surveyed points for a total of 1932 locations utilizable for ground measurements and canopy characterizations. The field areas consisted of 36 permanent poles drilled into ground positions measured with a distometer with exactly 10 m horizontal (± 1 cm) spacing from each other creating a 50 m × 50 m grid. A fixed line was attached to all poles and 2 m intervals were manually measured and marked between each. A differential GPS was used (±20 cm) at each of the poles to convert the projected coordinate system to a global one. The global coordinates were then distributed to all internal marked points for a final maximum rectification error of ±50 cm for each of the 1932 points. Two open field sites with 50 measurements points each (±20 cm) were also equipped as reference sites for direct comparison to the under canopy snow measurements (see Figure 1).

2.2. Snow Measurements

Snow depth data were manually collected after every storm with a total open area snowfall amount of 15 cm or greater in the winter 2012 and 2013 seasons. These measurements were collected at each forested point (1932 points) as well as at 100 open area control points (total of ∼69,000 measurements). Indirect snow interception measurements were collected when conditions allowed (Table 1). In some cases, a crust formed over the previous layer before the subsequent snow storm. In these cases, it was possible to measure the newly fallen snow from the base of the underlying crust. These differential snow depth measurements were made during nine storm events (Table 1) when the appropriate preconditions allowed: (1) forest canopy must be 100% snow free before a storm event, (2) minimal wind redistribution during the storm period, and (3) obvious crust on prior snow layer. These measurements were taken immediately after the storm period was over in order to reduce, as much as possible, snow unloading. These assumptions allowed the differential snow depth measurements to be thought of as 1-snow interception, and were easily converted to interception within the sample areas (storm interception = newly fallen snow in the open − differential snow measurement in forest). The indirect storm interception measurements were subsequently parsed in order to remove any potential conflicts with the necessary initial conditions and assumptions leaving ∼9000 interception measurement points available for use.

2.3. LiDAR Data

2.3.1. Technical Details

LiDAR data acquisition was carried out from the 11 September to 15 September 2010 using a Riegl LMS Q 560 sensor from a series of helicopter flyovers at a nominal flying altitude of 700 m for a total area of ∼90 km^2. The wavelength emitted from the Riegl device was 1550 nm with the pulse durations of 5 ns and up to 7 returns were detected per pulse using a maximum scan angle of ±15°. The postprocessing of the full waveform data set yielded an average echo density of 35.68/m^2 of the flyover domain and 19.05/m^2 for the last returns (i.e., shot density) within the utilized domain area. The affiliated digital terrain model (DTM) or the underlying ground surface elevations were computed by using the classified ground returns at a 0.5 m horizontal resolution by Toposys using their in-house processing software, TopPit (http://www.imagemaps.com/toposys.htm).

2.3.2. Polar System Elements

LiDAR data were used to characterize the canopy at all measurement points in the field areas. Using the method of *Moeser et al*. [2014], the classical canopy descriptors, LAI and canopy closure were derived from a transformation of the ALS data into a spherical coordinate system (Figure 2, bottom row). The ALS data were then flipped on the east west theta axis to represent an angular ground perspective. These data were converted in order to mimic hemispherical photos and further analyzed in a standard image analysis program, "Hemisfer" [*Schleppi et al*., 2007; *Thimonier et al*., 2010]. Potential incoming solar radiation (PISR) and the affiliated direct and diffuse components were also estimated from this process. In this manner, LAI and CC were estimated with significantly higher correlations that using the standard Cartesian approach (r: 0.93

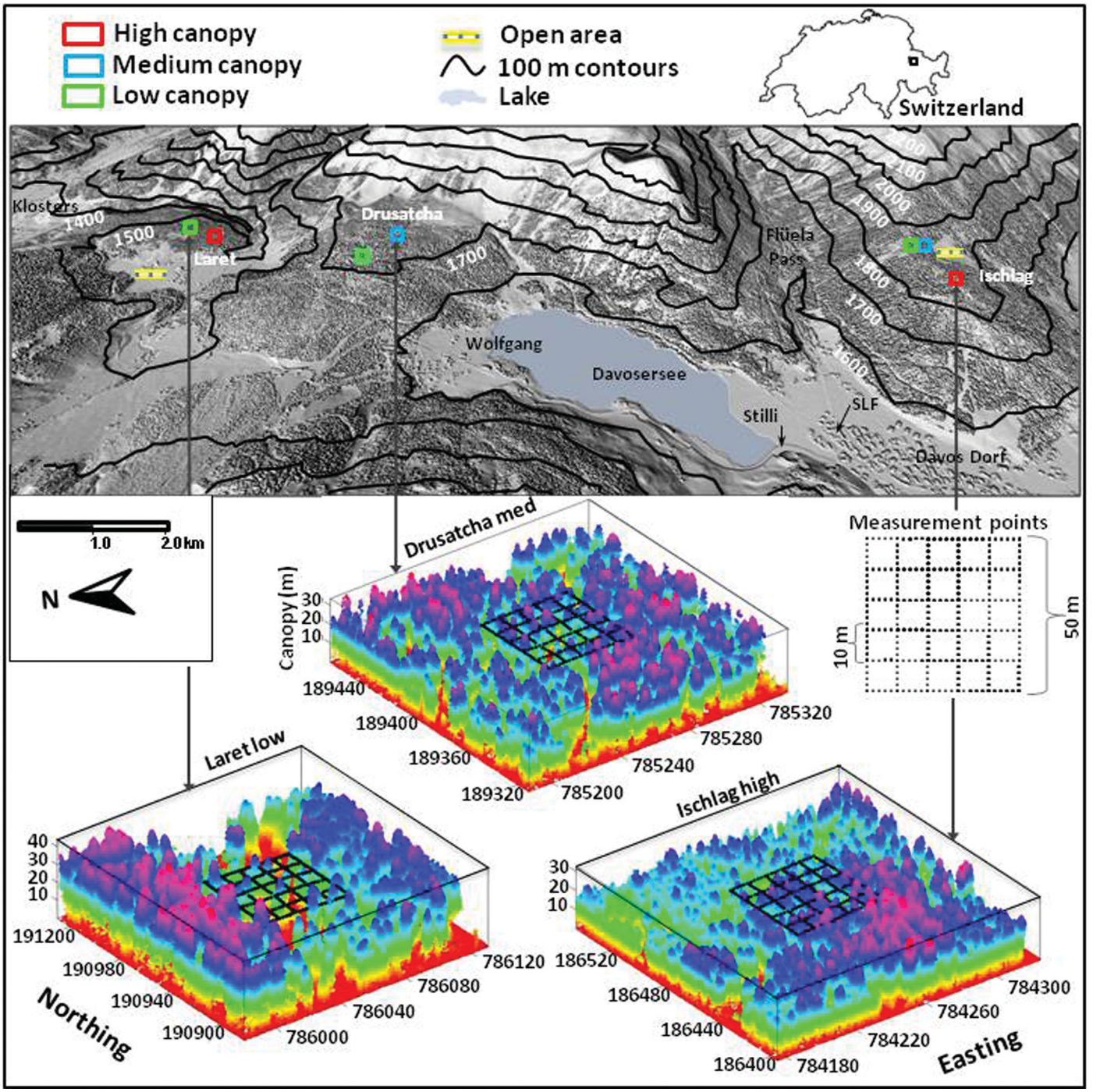

Figure 1. There were seven forested areas and two open field areas located in three elevation regimes around Davos in eastern Switzerland. Each field area was located in a unique gap fraction regime and maintained heterogeneous canopy characteristics. The box plots below the map are LiDAR cloud representations of three of the seven areas. The measurement points (276 points) surveyed in a 50 m × 50 m grid can be seen within each of the box plots. The remaining field areas maintained the equivalent experimental setup.

and RMSE: 0.037 for CC and r: 0.83 and RMSE: 0.813 for LAI). PISR showed similarly high correlations ranging from 0.90 to 0.94 dependent upon the field site. For details please refer to *Moeser et al*. [2014].

2.3.3. Cartesian System Elements

A series of novel canopy descriptors were created from the ALS data for all snow sampling points from a vector searching algorithm. The algorithm searched the LiDAR data transformed into a two-dimensional tree height model from a predefined center location approximately every 2° on the planar surface. The tree

Table 1. Dates of Snow Sampling Within the 2012–2013 and 2013–2014 Winter Seasons[a]

Storm Sate	Snow Depth (cm)	SWE (mm)	Temp (°C)
13 Jan 2013	28.53	22.65	−3.9
22 Feb 2013	20.31	13.89	−12.1
6 Mar 2013	37.16	28.96	−4.2
20 Mar 2013	16.81	13.62	−3.5
27 Mar 2013	17.41	12.81	−5.7
15 Jan 2014	27.65	24.42	−2.4
28 Jan 2014	27.80	21.18	−4.7
17 Feb 2014	24.31	22.49	−1.9
24 Mar 2014	35.88	26.93	−5.1

[a]The snow depth measurements represent the total snow storm depth which fell in the Laret open field site. The remaining values, representing storm-based values (SWE—total storm SWE and temp—average storm temperature, °C), are modeled.

height model was searched in 192 unique directions (∼every 2°) from vectors which originated from the predefined point. The vectors traveled in unique planar directions and did not stop until a canopy element from the tree height model was hit. Each vector was then given a distance (m) from the origin to the closest canopy element which was in the directional path of the vector (end point). The end points of each vector were connected and a two-dimensional polygon was created. This shape (m^2) represents the total open area around a point and is referred to as total gap area (see the top left tile of Figure 2 for an example of total gap area). The mean vector length (mean of the 192 vectors), which is called mean distance to canopy (m), was analyzed as well as the minimum (min distance to canopy), and maximum (max distance to canopy).

Statistics from the total gap area (m^2) were also analyzed. The mean gap diameter (m) was defined as the mean diameter of the gap area. The max gap diameter (m) or the maximum fetch of the total gap area as well as the minimum (min gap diameter) were also calculated. The distance to canopy estimates (mean distance to canopy, max distance to canopy, min distance to canopy) were also calculated for 180° and 90° directional windows (north, south, east, west, northeast, southeast, southwest, and northwest). For example, a 180° search window of south searches all vectors from 90° (due east) to 270° (due west) and a 90° search window of south searches all vectors from 135° (southeast) to 225° (southwest).

A secondary domain with a 10 radius around each predefined point was used. Within these domains, basic tree height proxies were estimated. Max canopy height, or the maximum height of the canopy elements within the domain as well as the mean canopy height, or the mean or all canopy elements within the domain were also calculated. A total of 57 canopy predictors were created from the vector searching algorithm automatically at each point. Table 2 displays all estimated canopy metrics. For a detailed method description refer to *Moeser et al*. [2015].

2.4. Data Analysis

2.4.1. Snow Depth to SWE Conversion

In following with the methods utilized by *Hedstrom and Pomeroy* [1998] and *Schmidt and Gluns* [1991], the model from the *US Army Corps of Engineers* [1956] was utilized where snow density was related to the average storm temperature as follows:

$$\text{snow density} = 67.92 + 51.25\ e^{(T/2.59)} \quad (1)$$

where T is average storm air temperature (°C). The air temperature at each site, for each storm event, was interpolated based on an altitudinal gradient derived from surrounding meteorological stations. The interpolation utilized temperature data from four meteorological stations from the "Intercantonal measurement and information system" (IMIS) surrounding Davos, Switzerland, at four unique elevation bands: 1560, 2140, 2290, and 2540 m (IMIS-KLO, IMIS-SLF, IMIS-PAR, and IMIS-WFJ).

Equation (1) was then used to attach fresh snow density values to all measured snow depth values at each storm to arrive at SWE. Finally, the interception measurements were calculated from a simple subtraction of the freshly fallen SWE in the open − freshly fallen SWE in the forest.

2.4.2. Interception Model

In accordance with the prior research from *Satterlund and Haupt* [1967] and *Schmidt and Gluns* [1991], an initial increase in interception efficiency until an optimum (I_{max}) was reached along with a subsequent falling limb was seen within the plotted efficiency values at all canopy densities within this data set (Figure 7). Due to this, the sigmoid growth curve proposed by *Satterlund and Haupt* [1967] was used as the underlying model within this study:

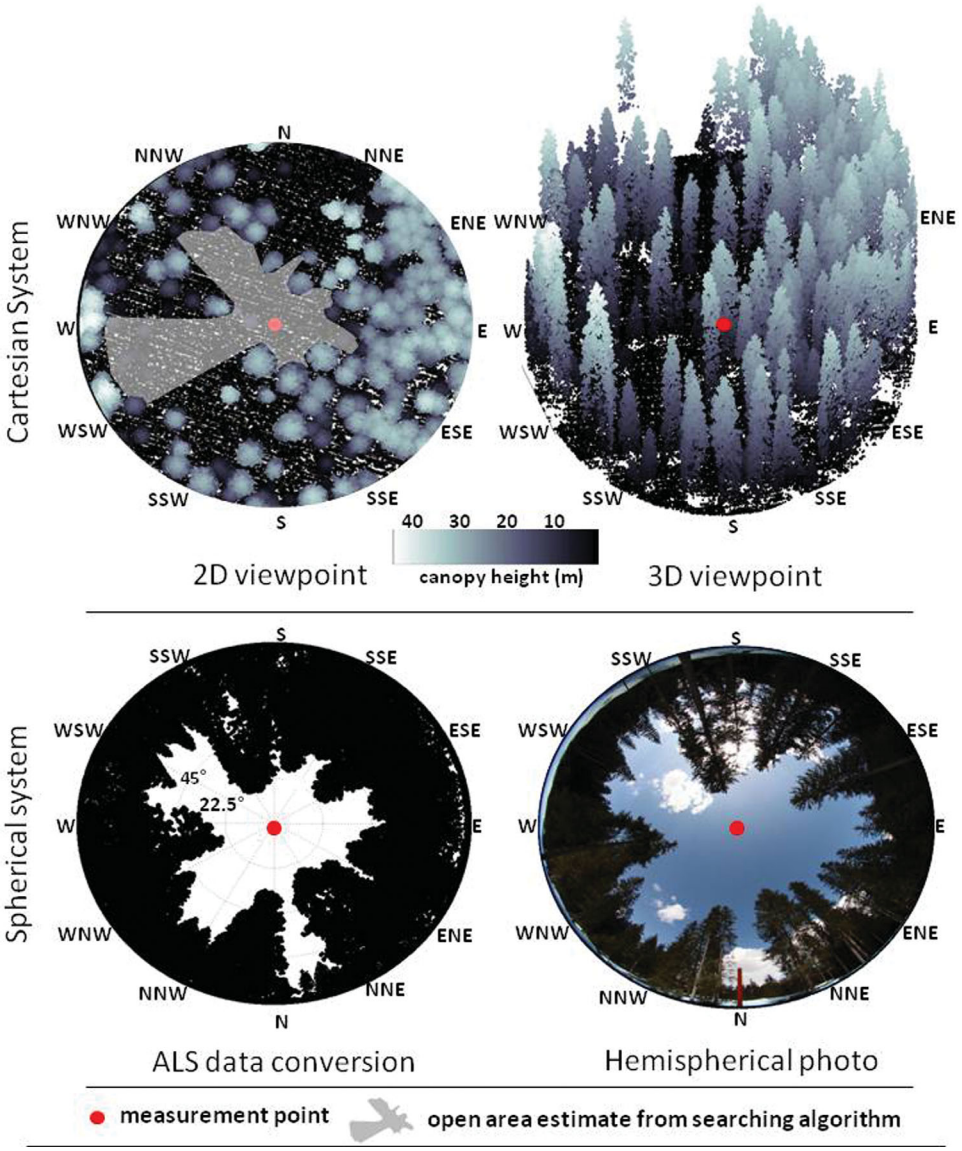

Figure 2. The LiDAR data are displayed in the standard downward looking Cartesian viewpoint on the top row with an average echo density of 36 points/m^2. (top left) Displayed in a two-dimensional format, includes an example of a polygon created from the vector searching algorithm. From these polygons, a variety of statistics can be estimated such as mean distance to canopy and total gap area. (bottom left) An example of LiDAR data converted to mimic a hemispherical image from an angular upward looking viewpoint. (bottom right) An actual hemispherical photograph. All images have been derived from the same point within an open area at the Laret low field area and have a data trap size of 100 m (100 m radius around point).

$$I = \frac{I_{max}}{1 + e^{-k(P - P_0)}} \tag{2}$$

where I is interception, I_{max} is the interception storage capacity (called S in prior studies), P is the storm precipitation, P_0 is the accumulated storm accumulation at the time of maximum interception efficiency, and k expresses the efficiency rate. In prior studies, the factors I_{max}, k, and P_0 were derived on a storm and tree species basis. *Hedstrom and Pomeroy* [1998] furthered this work by calculating I_{max} for trees from empirical values suggested from *Schmidt and Gluns* [1991], derived from snow density:

$$I_{max} = 0.27 + \frac{46}{\rho_{snow}} \tag{3}$$

where ρ_{snow} is the density of fresh snow and multiplied this with LAI. *Hedstrom and Pomeroy* [1998] also used a static multiplier of 5.9 to this equation for spruce trees and defined interception as:

Table 2. Table Modified From *Moeser et al.* [2015][a]

Canopy Descriptors	The Full Domain (360°)	180° Sector (N, S, E, W)	90° Sector (N, S, E, W, NE, SE, SW, NW)
Total gap area (m^2)	√	√(4×)	√(8×)
Max gap diameter (m)	√		
Max distance to canopy (m)	√	√(4×)	√(8×)
Min gap diameter (m)	√		
Min distance to canopy (m)	√	√(4×)	√(8×)
Mean gap diameter (m)	√		
Mean distance to canopy (m)	√	√(4×)	√(8×)
Max canopy height proxy (m)	√		
Mean canopy height proxy (m) (m)	√		

[a]Fifty-seven canopy metrics were created from the searching algorithm. Gap area and distance to canopy metrics were derived for the entire domain as well as for each directional sector from a 90° and 180° search window. The gap diameter metrics and canopy height proxies were generated only for the entire domain. Values within parentheses indicate number of times the descriptor was created.

$$I = 0.678 * I_{max} * \left[1 - e^{\frac{-CC*P}{I_{max}}}\right] \quad (4)$$

where 0.678 is a snow unloading multiplier valid for time after snow fall of 0–7 days.

The interception data set was randomly divided into a calibration and a validation data set of 80% and 20% of total respectively. The I_{max} was calculated from a direct comparison of interception measurements from the calibration data set at the maximum efficiency event (13 January 2013) to all potential predictors (forest metrics). This included all parameters seen within Table 2, plus LAI, CC, incoming solar radiation as well as storm temperatures and fresh snow density. The parameters were then intercompared using a correspondence analysis (CA) and k-means clustering analysis pairing in order to better understand how each of the variables related to each other.

2.4.3. Model Construction

CA is a nonparametric principle components style analysis method specifically used for analyzing correspondence (or independence) among variables. This analysis has distinct advantages over traditional factorial analyses in cases where the analyzed data scales have a small response ranges. Within CA, the significance of data pairings is based upon the chi-squared distance between the actual and expected values [*Car*, 2002]. CA transforms the data into an "equivalent" data space where the largest amount of data variability is captured within the first dimension (displayed as the *x* axis) the subsequent largest amount of variability in the second dimension (displayed as the *y* axis) and so on.

Each dimensional axis can further be given a significance value which represents the amount of variability the dimension (or axis) represents from the data set (percent of inertia). Independence can therefore be qualitatively visualized by the separations distance between the plotted potential predictors (canopy metrics, etc.) with greater significance given to separation distances seen on the axes with higher percent of inertia values. Specifically, small distances between points indicate a high association (cross correlation) and large distances indicate low association or independence. For a full mathematical description please see: *Car* [2002], *Greenacre and Blasius* [1994], *Lorenzo-Seva et al.* [2009], *Van de Velden and Kiers* [2005].

In order to reduce the potential bias in visual (qualitative) approaches such as CA, k-means clustering was used in order to quantify and automate the variable separations seen within the output of CA. k-means clustering was used to automatically choose groups of variables (canopy metrics) which plot similarly on the CA graph (Figure 4) by maximizing their intercluster distances and minimizing their intracluster distances [*Seber*, 1984; *Späth*, 1986]. The factor values (percent of inertia values) were integrated into the k-means routine and the routine was performed iteratively on the data set where the centroid of each potential data cluster (grouping of variables) was randomly chosen. From prior work with similar data sets (interception ratio), the number of cluster groupings (k) was set to 4 [*Moeser et al.*, 2015].

The component with the highest correlated value from each of the groupings was then used within a flexible regression modeling program. The program was fully automated and used the output of the CA/k-means clustering routine as input from the calibration data set. The program created a series of regressions for one variable, two variables, three variables, and four variables with potential outputs being a (1) linear model, (2) linear model with component interaction, (3) quadratic model, and (4) quadratic model with component interaction. The input format of the variables was allowed to change between normal and log normal. This allowed for 16 potential models for one input variable, 112 potential models for two input variables, 96 potential models for three variables, and 60 potential models for four variables for a total of 284 potential models. The program chose the best fit for each model scenario (one variable model, two variable model, three variable model, and four variable model) based on the lowest RMSE. The best fit I_{max} model

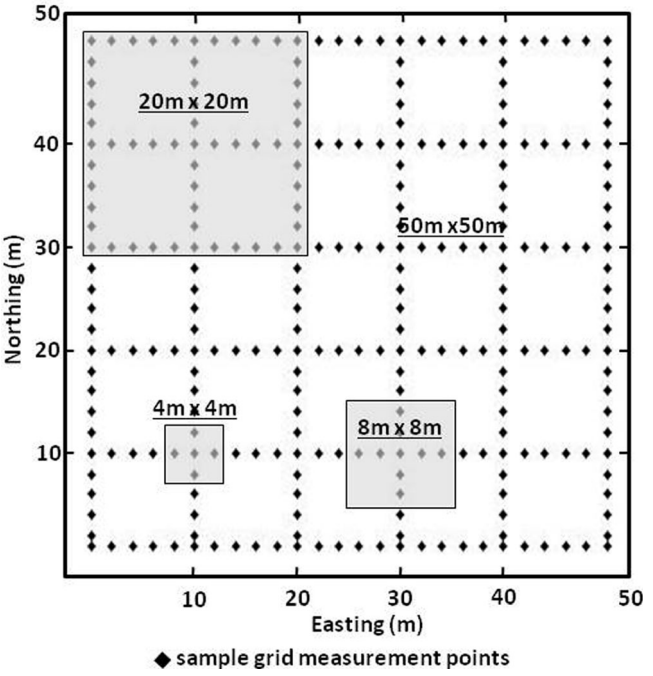

Figure 3. Represents an idealized sampling grid (276 points) and grid cells. The grid cells were created in order to avoid any sample point sharing between grid cells. The 4 m × 4 m grid cells contained five measurement points for a total of 16 per field area, the 8 m × 8 m grid cells contained nine points for a total of 16 per field area, the 20 m × 20 m grid cells contained 67 measurements points for a total of 4 per field area, the 50 m × 50 m grid cells contained 276 points, and the 250 m × 250 m grid cells, which was a composite of five field sites, contained 1380 points.

scenario was then manually chosen from an analysis of the RMSE, correlation, visual analysis of the residuals, and deviation of fit on the 1:1 line.k and P_o were also subsequently optimized using the same method described above where k and P:

$$k = -\frac{\ln\left(\frac{Imax}{I} - 1\right)}{P - P_0} \quad (5)$$

$$P_o = -\frac{\ln\left(\frac{Imax}{I} - 1\right)}{-k} + P \quad (6)$$

However, due to extremely low correlations of k and P_0 to any of the variables, these values were also used as constants. Equation (2), with the integration of the new I_{max} model, was explicitly solved from a series of given input values for k (between −1 and 1) and P_0 (between minimum and maximum P SWE values) where the optimized values were derived from the minimization of the RMSE of the estimated and actual interception values from the calibration data set.

2.4.4. Model Upscaling

It is possible interception simulations based on a single model run using averaged canopy parameters over a grid area could be systematically offset as compared to interception averaged over individual point-based model runs using local canopy parameters. In efforts to reduce the potential of systematic bias upscaling from a point to larger scales, a stratified model approach was also integrated into the model.

For upscaling from a point to a grid, the domain was split into a series of grid cells ranging from 16 to 62,500 m^2, where all internal measurement points within each grid cell were averaged. The grid sizes were chosen in order to avoid any overlap or sharing of internal grid points to neighboring grid cells of the same size. See Figure 3 for an idealized representation of a field area and the grid domains. The 16 m^2 grids included five internal measurements points within each grid for a total of 575 grids utilized for this study, the 64 m^2 grids contained nine points with a total of 575 grids utilized, the 200 m^2 grids contained 67 points with a total of 143 grids utilized, the 2500 m^2 grids contained 276 points with a total of 35 grids utilized, and the 62,500 m^2 grids contained 1380 points with a total of nine grids utilized.

The same approach was utilized as outlined above (section 2.4.3) to create the stratified model except the regressions were further parameterized using two threshold values governed by a canopy parameter. For example, if LAI was chosen as the parameter, with the threshold values being 3 and 5, the modeling domain would therefore be clustered into three zones (1) $LAI \leq 3$, (2) $3 < LAI < 5$, and (3) $LAI \geq 5$ where a separate model would be utilized for grids or points in each of the three zones.

In order to choose the correct parameter as well as the threshold values of that parameter, dummy variables were integrated into the regression analyses which were given values of either 0 or 1, dictated by the two threshold values. A list of the threshold value pairs were automatically created by the program by first separating the range of the utilized parameter values into a series of equidistant step values (up to 100). These values (threshold one) were attached to a value from the same list of step values as long as the step size was greater than the first threshold (threshold two). For example, if LAI was used and ranged from an LAI of 1 to an LAI of 4, the equidistant step would range from 1 to 4 and the threshold pairs would be,

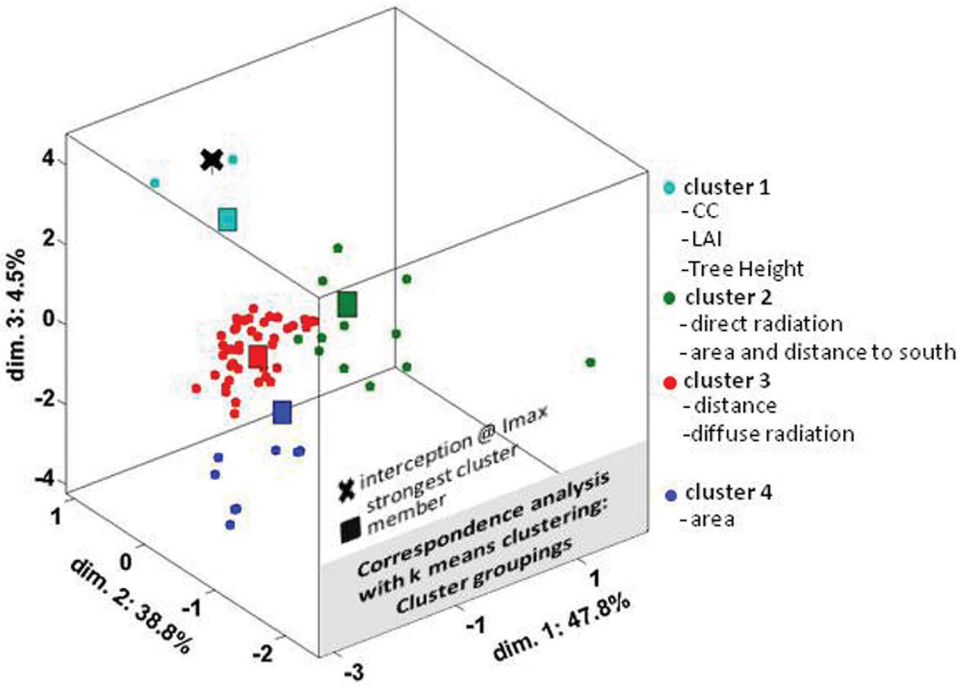

Figure 4. The parameter groupings within the correspondence analysis were chosen by k-means clustering with each group labeled by color. Each box within the colored grouping shows the highest correlated element within the grouping. The highest ranking member of group 1 was canopy closure (R: 0.76), group 2 was mean distance to canopy (R: 0.83), group 3 was daily average PISR (R: 0.71), and group 4 was total open area (R: 0.76). The cross represents the location of the independent element, snow interception at maximum efficiency.

1,2:1,3:1,4:2,3:2,4:3,4. If the threshold pair, was 1,3: then the domain would be clustered into three zones: (1) LAI ≤ 1, (2) $1 <$ LAI < 3, and (3) LAI ≥ 3. Two extra variables (dummy variables) would be used within the regressions, with the first variable displayed as 1 when LAI was $\geq$1 and 0 when LAI was $<$1 and the second variable displayed as 1 when LAI was $\geq$3 and 0 when LAI was $<$3.

The best fit threshold pair was optimized from a minimization of the RMSE when each regression run that utilized the threshold pairs was analyzed. The canopy parameter was also left flexible, where the program, as with the threshold values, also chose the best parameter based on an RMSE minimization. When the best fit run was found, the regressions were decomposed based upon the dummy variables giving unique equations for each range (three equations for two thresholds).

3. Results and Discussion

3.1. Model

3.1.1. Canopy Parameter Analysis

The generated canopy parameters varied greatly through space. For example, LAI varied from $\sim$1.2 to 8.0 and total gap area varied from $\sim$0 to 2270 m^2. Figure 4 shows the CA/k-means clustering analysis of all canopy parameters. The traditional canopy descriptors, LAI and CC along with mean tree height showed a high degree of cross correlation (cluster one) and the strongest member (highest correlation to interception at I_{max}) was canopy closure (R: 0.76). The next smallest cluster grouped all area (total gap area, gap area to the north, gap area to the northeast, etc.) estimates except those which had a southerly direction, with the strongest end-member being total gap area (m^2) (R: 0.76). The next cluster contained all direct incoming solar radiation components as well as distance to south and area to the south estimates with the strongest member being average daily PISR (R: 0.71). The largest cluster included all distance estimates except those to the south and diffuse incoming radiation estimates with the strongest end-member being mean distance to canopy (m) (R: 0.83). Contrasting with the use of fresh snow density in the model framework (equation (3)) utilized by both *Schmidt and Gluns* [1991] and *Hedstrom and Pomeroy* [1998]; fresh snow density showed extremely low correlations (along with storm temperature) within this data set. Due to this, these parameters were not

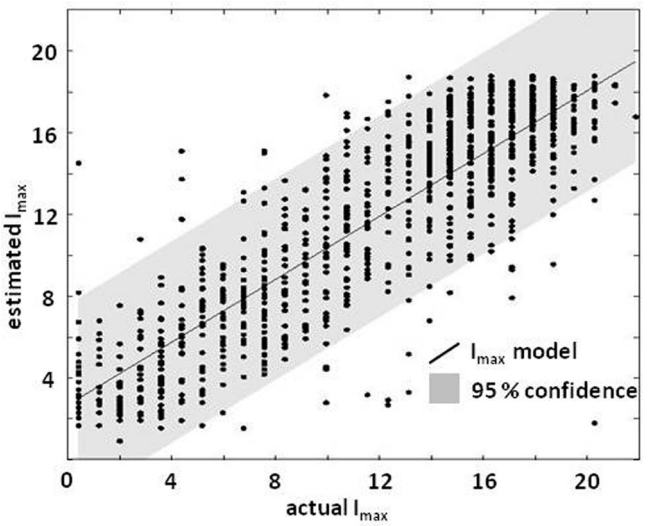

Figure 5. Compares I_{max} estimated from the model with the actual I_{max} values from the 13 January 2013 storm event. The model is represented as a black line with an RMSE of 2.82 mm SWE, and an r^2 of 0.75 (R: 0.86). The 95% confidence interval of the model is seen as gray shading.

included in the CA/k-means clustering analysis ($R < 0.10$). The correspondence/k-means clustering analysis gave similar results from prior analyses of all parameters to interception ratio (differential snow measurement in forest/newly fallen snow in the open). For a thorough results analysis of the CA/k-means in regards to interception ratio, see *Moeser et al.* [2015].

3.1.2. I_{max}

I_{max} was best estimated from the integration of three variables obtained from the aerial LiDAR data, (1) mean distance to canopy (m), (2) canopy closure, and (3) total gap area (m^2) with an RMSE of 2.82 mm SWE, and an r^2 of 0.75 (R: 0.86). See Figure 5. The integration of the fourth cluster grouping from the CA analysis (PISR) added little skill to the final model and was subsequently omitted. Mean distance to canopy was created from the vector searching algorithm and represented the average distance to the closest canopy feature. Total gap area was also created from the vector searching algorithm and was an estimate of the total gap area from the perspective of the measurement point. Canopy closure was derived from conversion of the ALS data into a spherical coordinate system in order to create synthetic hemispherical photographs. The I_{max} model and affiliated coefficients are shown in equation (6) and Table 3. The I_{max} values within this study are considerably higher than in the prior works of *Satterlund and Haupt* [1967] and *Schmidt and Gluns* [1991]. However and as noted in these papers, extrapolating results from branches and saplings to trees should exhibit increases in I_{max} values primarily from increased snow bridging effects from higher snow particle drop-off from upper to lower branches.

The I_{max} model proposed by *Hedstrom and Pomeroy* [1998], utilized LAI as a multiplier to equation (3) along with a static multiplier of 6.6 (for spruce trees). However the CA/k-means analysis showed reduced correlation when LAI (R: 0.58) was directly compared to interception as with CC to interception (R: 0.76). Correlations of snow density to interception were also minimal. This implies that at least when storm based I_{max} is estimated, (1) CC gives better estimations of I_{max} than that of LAI and (2) the surrounding canopy elements appear to play a larger factor on I_{max} than the density of the falling snow.

$$I_{max} = m1(x1) + m2(x1)^2 + m1(x2) + m2(x2)^2 + m1(x3) + m2(x3)^2 + b \quad (7)$$

3.1.3. Interception

k and P_0 had negligible correlations to all canopy parameters as well as to storm temperature and snow density (equations (4) and (5)). Due to this, the k and P_0 were optimized from a minimization of the RMSE to 0.3 and 13.3, respectively.

Table 3. I_{max} Was Derived From the Highest Efficiency Storm Event (13 January 2013) and is Represented as a Quadratic Equation With the Independent Variables Described From Aerial LiDAR Data[a]

	Variable (log)	m1	m2	b
x1	Mean distance to canopy (m)	2.167	−3.410	20.819
x2	Canopy closure	55.761	181.858	
x3	Total open area (m^2)	−2.493	0.499	

[a]Each variable was transformed using the natural log. I_{max} has units of mm SWE.

Interception is therefore:

$$I = \frac{I_{max}}{1 + e^{-0.3(P-13.3)}} \quad (8)$$

where I is interception in mm and I_{max} is equation (6). The model can be used at substorm event time scales from integration of the underlying efficiency distribution. Therefore, P can

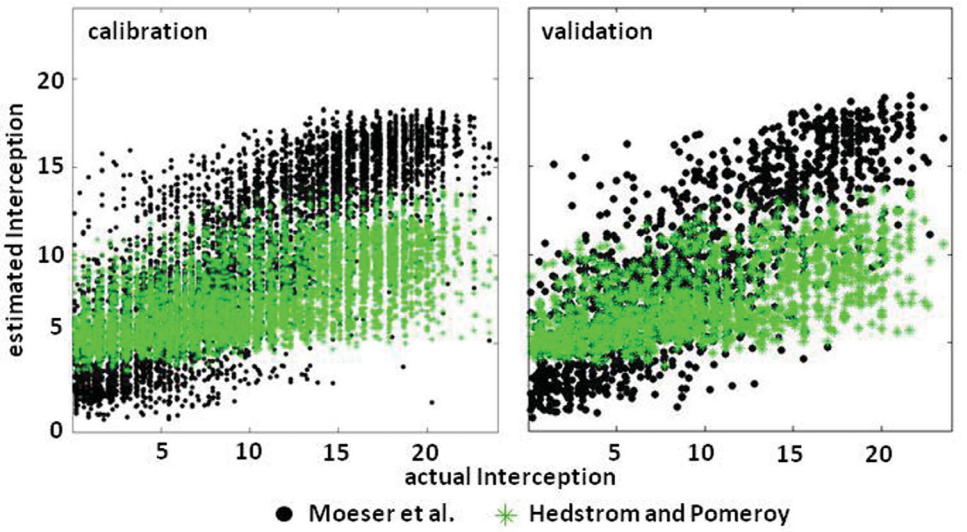

Figure 6. Performance comparison of the proposed interception model [*Moeser et al.*] to the model by *Hedstrom and Pomeroy* [1998]. (top left) The calibration data and (top right) the validation data showed similar trends. The Moeser et al. maintained an r^2 of 0.65/RMSE of 3.39 mm SWE, from the calibration data, and an r^2 of 0.64/3.4 mm SWE, RMSE in the validation data. The Hedstrom and Pomeroy model showed an r^2 of 0.39/RMSE of 5.19 mm SWE, within the calibration data and an r^2 of 0.41/5.18 mm SWE, RMSE in the validation data showed a substantial interception underestimation in both data sets.

be input at each time step as a summation of precipitation from when $I > 0$ (start of storm period). However, this model was created from data collected immediately after storm events, it inherently integrates unloading that occurs during the storm event. Due to this, such a model should not be used in tandem with an unloading function during storm events.

The model fit both the calibration and validation data sets well with an r^2 ranging from 0.64 to 0.65 (R: 0.81) and an RMSE from 3.39 to 3.4 mm SWE (Figure 6). The sigmoidal shaped efficiency model distribution (left tile, Figure 7) shows a good fit with the actual data from each storm event (Figure 8).

The *Hedstrom and Pomeroy* model showed an r^2 ranging from 0.39 to 0.41 for the calibration and validation data sets as well as an RMSE ranging from 5.18 to 5.19 mm SWE. This model showed a severe interception underestimation with estimated interception values over ~5, with the opposite holding true for values under this range. This is most likely due to the underlying efficiency distribution inherent within this model, which does not apply to this data set. Figure 7 exhibits the basic distribution differences between the two

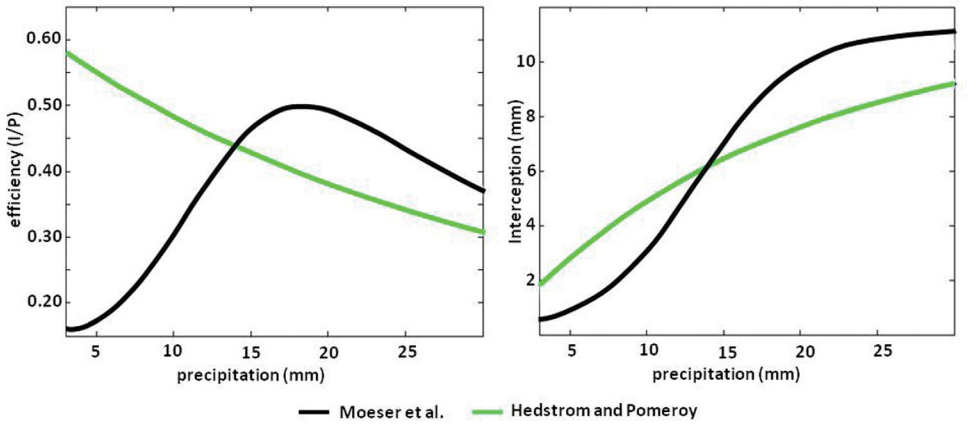

Figure 7. Comparison of interception model estimation distributions using mean canopy values and a precipitation data series from 1 to 30 mm with a 0.1 mm step. The Moeser et al. model is seen in black and showed an initial exponential increase in efficiency before decreasing. The Hedstrom and Pomeroy model (in green) showed an exponential decrease in efficiency starting from zero. The Moeser et al. interception model showed an exponential increase (with the highest slope at P_0) until I_{max} was reached at which point estimates level. The Hedstrom and Pomeroy showed increasing interception estimates with a slow reduction in slope until a maximum is reached.

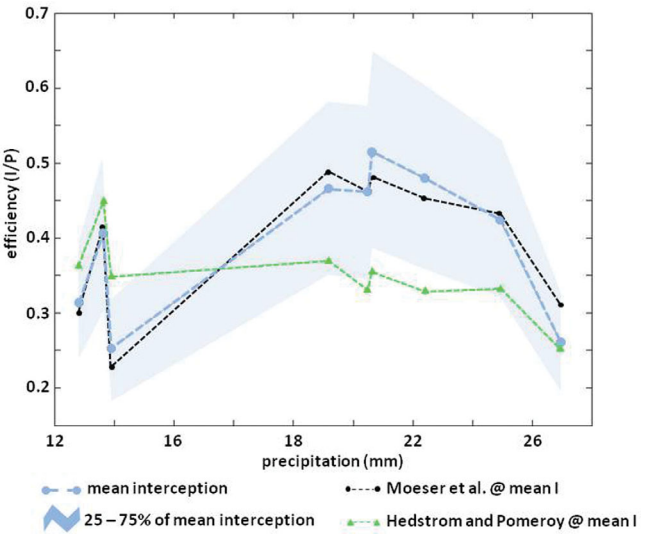

Figure 8. Comparison of measured interception efficiency from the nine storm events (Table 1) where mean efficiency from each event is shown in dark blue circles. The efficiency values ranging from 25% to 75% of mean interception are shown as a light blue band. Mean modeled efficiency values from the Moeser et al. model are shown as small black circles. The mean values from the *Hedstrom and Pomeroy* model are shown as green triangles. Note that the large mean efficiency underestimation from the *Hedstrom and Pomeroy* model.

models. The Hedstrom and Pomeroy demonstrated an exponential decay of the efficiency from the beginning of snow fall, whereas the Moeser et al. showed an initial increase in efficiency until I_{max} was reached, at which point the efficiency dropped exponentially. These differences were especially visible when the interception efficiency from the models were compared to the measured efficiency from each of the storm events (Figure 8).

3.1.4. Parameter Analysis

As noted in section 3.2.2, the *Hedstrom and Pomeroy* [1998] model utilized LAI as a principle parameter to estimate I_{max}. This is further integrated within the interception model and used as a divisor to CC and precipitation for the exponential decrease portion of the model [*Hedstrom and Pomeroy*, 1998; *Pomeroy et al*., 1998a, 1998b]. However, when used with this data set, the paring of these two parameters (LAI, CC) could cause potential cross correlation within the model (see section 3.2.1) highlighting the necessity of parameters which describe varying aspects of the overstory.

Each independent canopy parameter within the Moeser et al. interception model (mean distance to canopy, canopy closure, and total gap area) was visually analyzed for sensitivity to I_{max}, efficiency, and total interception (Figure 9). Mean distance to canopy showed the highest skill, with high correlations and low variance for the entire data series. Canopy closure demonstrated higher correlations and lower variance for both high and low canopy closure values, with increased variance present within the median values. Total gap area maintained equivalent correlations. However, this parameter demonstrated a fairly distinct zone where the line slope changed and variance increased ($\sim$500–1000 m^2). The separation between interception $> I_{max}$ and interception $< I_{max}$ showed no significant mixing until mean distance to canopy was $\sim$greater than 18 m. Interestingly, this threshold came much sooner in the data range of canopy closure ($\sim$less than 0.92) and total open area ($\sim$greater than 250). This implies that the lowest efficiency ranges (where mean distance to canopy is high, total open area is high, and canopy closure is low) are best captured by mean distance to canopy. The independent variable correlations at I_{max} (equation (6)) showed no significant reductions when this was used within the interception model (equation (7)) also lending significance to the underlying sigmoidal model distribution curve.

3.1.5. Model Upscaling

When the modeling domain was stratified, the canopy parameter that demonstrated the lowest reductions in RMSE was total open area with the affiliated thresholds optimized at (1) 250 m^2 and (2) 750 m^2. This created a separate model for three open area zones: (1) total open area $\leq$250 m^2, (2) total open area $>$250 m^2 and $<$750 m^2, and (3) total open area $\geq$750 m^2. The independent parameters are the same as the point-based model (equation (6) and Table 3), with the same underlying quadratic format and natural log conversion of independent variables. However, the coefficients have changed for each parameter from the point-based equation. From a decomposition of the regression model, the dummy variables were removed giving unique intercept values for each open area group (Table 4).

The stratified model showed an improvement in the RMSE by a factor of 1.75–2.18 when compared to the *Hedstrom and Pomeroy* model at each grid scale. The standard deviation of the estimated interception was also higher by a factor of 1.95–2.17 within the Moeser et al. stratified model. These differences represented fairly substantial underestimations of interception as well significant spread in estimate confidence within

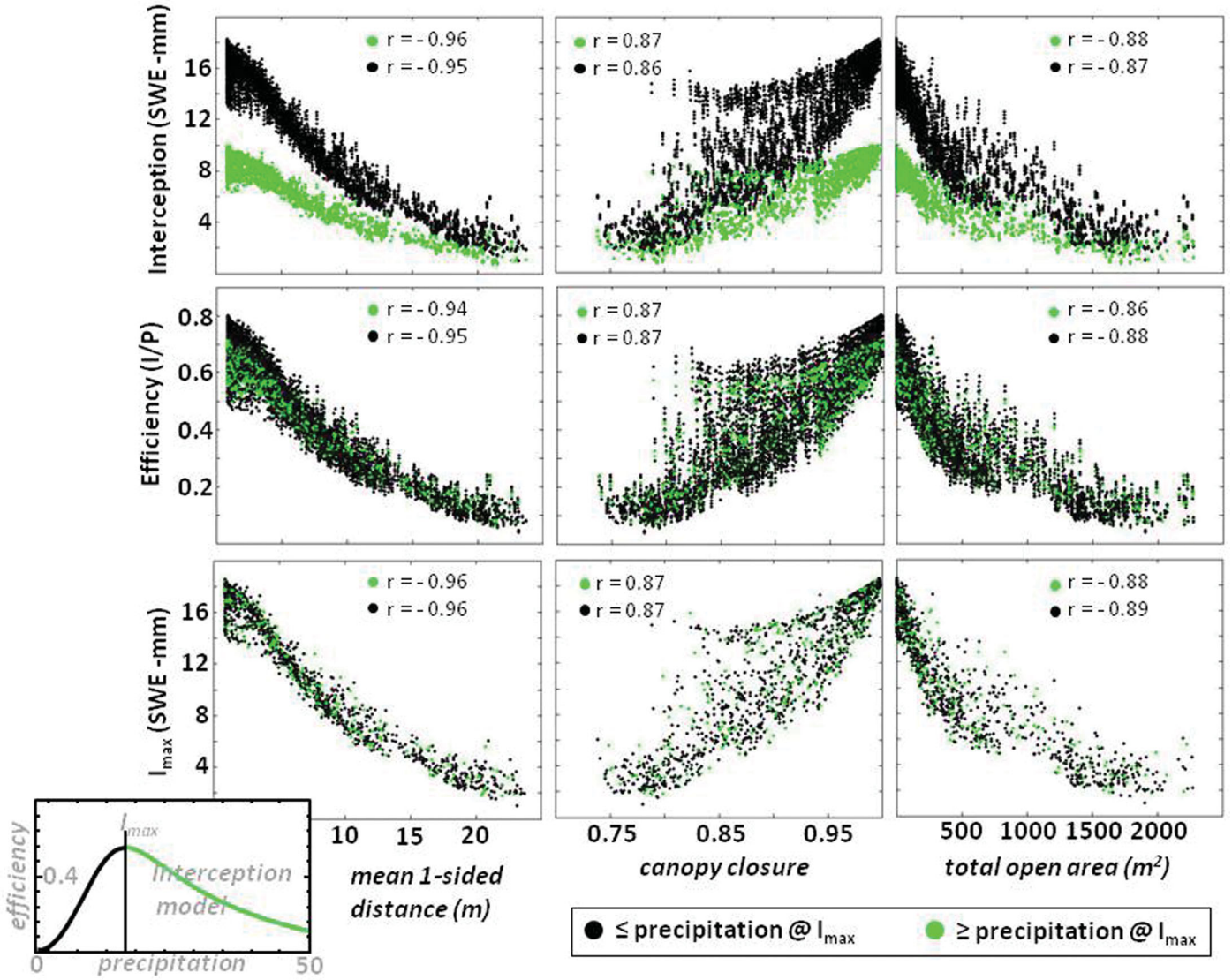

Figure 9. All dependent canopy parameters within the interception model showed high correlations to (top) interception, (middle) efficiency, and (bottom) I_{max} and each resolved high percentages of explained model variance. Mean distance to canopy was the most skilled variable within the model and maintained low internal variance and high correlations for the entire variable domain. Canopy closure retained the highest correlations and lowest variance at both high and low values with the median values showing the highest parameter variance. Total open area maintained a fairly uniform correlation. However, this parameter had a fairly distinct zone where parameter variance increased (500–1000 m^2).

the *Hedstrom and Pomeroy* model. However, both models showed an r^2 increase at each grid size, due to the smoothing of data (Figure 10).

When the point-based model was utilized for the grids, the results showed insignificant increases in the r^2 and RMSE (r^2: 0.65–0.66 RMSE: 3.39–3.38) as compared to the stratified approach. Despite this, increased variability of the data was captured within the stratified model, which slightly improved estimates at all scales. Figure 11 is a Taylor plot of the models: (1) Moeser et al. point model, (2) Moeser et al. model with a stratified approach, and the (3) *Hedstrom and Pomeroy* model at all scales. Due to the geometric relationships of the plotted statistics, the skill of the model can be quantified by both distance to the measured data as well as distance to the standard deviation lines of the measured data [*Taylor*, 2001]. The Pomeroy showed large underestimations for all grid sizes. The Moeser et al. point model showed smaller underestimates with improvements from the stratified approach at all scales.

3.1.6. Model Improvement: Efficiency Distribution Versus Canopy Structure Metrics

In order to differentiate how much of the modeled interception improvement was due to the use of canopy structure elements and how much to the sigmoidal interception distribution; we have created a model

Table 4. Model Coefficients and Intercepts for the Stratified Model[a]

			Intercept Values		
Variable (log)	m1	m2	(Open Area $\leq$ 250 m^2)	(250 $<$ Open Area $<$ 750 m^2)	(Open Area $\geq$ 750 m^2)
x1	1.275	−3.292	20.895	19.895	18.895
x2	53.324	169.895			
x3	−2.598	0.567			

[a]Equations (6) and (7) remain the same.

where I_{max} was estimated using just CC. The exact methodology that used in the prior models was implemented to create this comparative model, where I_{max} is:

$$I_{max} = 71.55(CC) + 64.39(CC)^2 + 17.71 \quad (9)$$

$$I = \frac{I_{max}}{1 + e^{-0.29(P-13.2)}} \quad (10)$$

where CC was log transformed and k and Po have been optimized to 0.29 and 13.2, respectively (equation (10)). The model was fit to both the calibration and validation data sets with an r^2 which ranged from 0.49

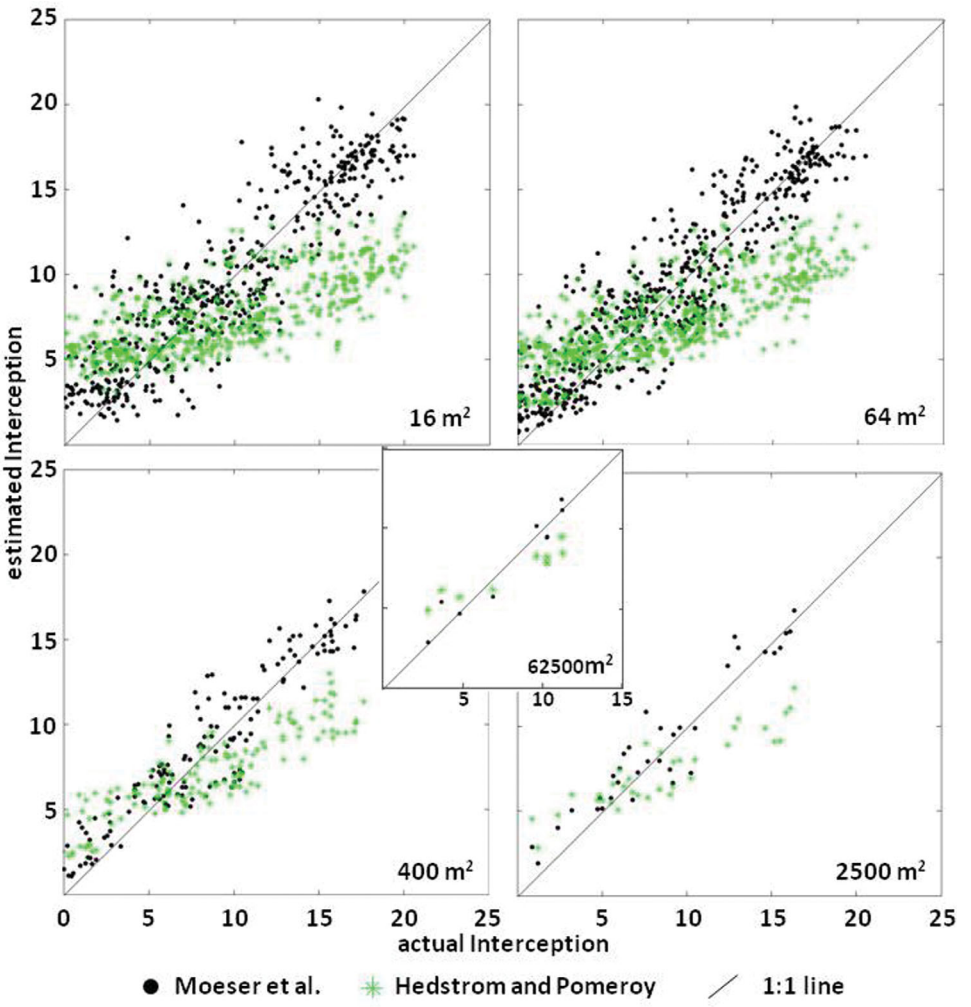

Figure 10. Comparison of the stratified model to the *Hedstrom and Pomeroy* model from 16 to 62,500 m^2 grid sizes. While each model displayed an improved fit as the grid size increased, the *Hedstrom and Pomeroy* model demonstrated a significant underestimation at all grid sizes. See Table 5 for a list of general statistics of each model. The point model derived similar results as to the stratified model.

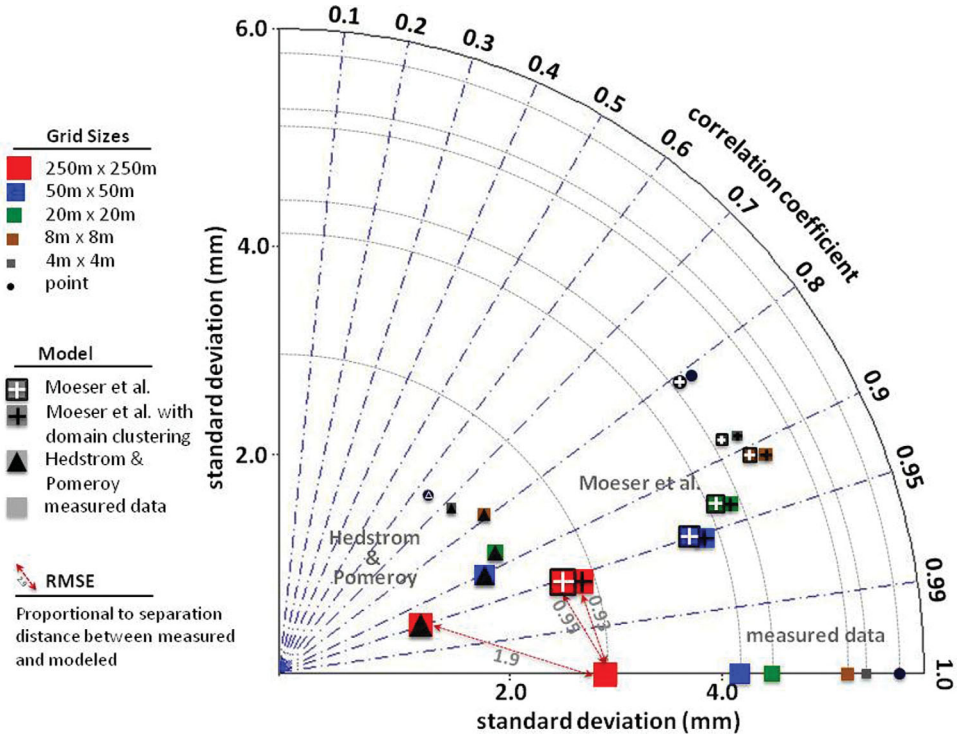

Figure 11. Taylor diagram comparing the: (1) Moeser et al. point model, (2) Moeser et al. model with a stratified approach, and (3) *Hedstrom and Pomeroy* model at the point scale and all grid sizes from 16 to 62,500 m^2. The standard deviation of the estimates and the actual data are plotted on the linear axes and represent the overestimation or underestimation of the models. Model estimates that plot to the right of the actual data (for the appropriate grid size) represent an overestimation and model estimates which plot to the left represent and underestimation. The correlation is plotted on the log scale axis. RMSE at each grid size is directly proportional to the distance away from the actual data. The red arrows between the 62,500 m^2 grid series show the distance: RMSE relationship, with the RMSE values labeled in light gray. The Moeser et al. models showed improved skill at all grid sizes. The stratified approach, while showing negligible improvement in RMSE or correlation, showed slight improvements in estimation power from an improved representation of the data sets variability and resulted in smaller underestimations.

to 0.53, and an RMSE of 3.96 for both data sets. This implies that for the calibration data set, ~48% of the improvement in the r^2 and ~67% of the improvement in RMSE, is due to the inclusion of canopy structure metrics (mean distance to canopy and total gap area). While it was not possible to fully separate the underlying model distribution and the variables, this shows that in general the improvement is due to both, the underlying sigmoidal distribution as well as the inclusion of canopy metrics which describe the overall canopy structure (mean distance to canopy and total gap area).

It should be noted that the *Hedstrom and Pomeroy* interception model was created in a cold boreal forest environment. Despite this, it is the only know model which the authors are aware which has been integrated into snow melt models which have a forest canopy module. This should emphasize that there may be a need for an alternative model which can better perform in other environments.

Table 5. Basic Statistics Comparing the Stratified Model and the *Hedstrom and Pomeroy* at Various Grid Sizes[a]

	16 m^2		64 m^2		400 m^2		2500 m^2		62,500 m^2	
	M et al.	H and P	M et al.	H and P	M et al.	H and P	M et al.	H and P	M et al.	H and P
r^2	0.78	0.52	0.85	0.62	0.86	0.76	0.91	0.82	0.91	0.89
RMSE	2.54	4.54	2.24	3.93	1.73	3.08	1.31	2.86	0.93	1.90
stdev	4.79	2.21	4.96	2.41	4.49	2.30	4.14	2.11	2.75	1.39

[a]The stratified model maintained an RMSE (mm SWE) approximately half that of the *Hedstrom and Pomeroy* for all grid sizes as well as a doubling of the standard deviation (mm SWE) at all grid sizes representing the estimation spread and subsequent underestimation of the *Hedstrom and Pomeroy* at all grid sizes. See Figure 10 for a visual representation.

4. Conclusion

Storm-based interception was accurately predicted across a large range of canopy closure and gap opening regimes (from 0 to 2250 m^2) from a database which included approximately 9000 manually measured interception points at 1237 independent points. The size and heterogeneity of both the calibration and validation data sets eclipses prior data sets utilized from interception modeling studies input data by over an order of magnitude. The model showed a good fit with increased performance dependent upon the grid cell size with r^2 values ranging from 0.65 at the point scale to 0.91 at the largest 62,500 m^2 grid scales. The RMSE showed a similar trend and ranged from 3.35 to 0.93 mm SWE.

The stratified model results showed modest improvements in interception estimations with the most obvious benefits being an increase in variation captured within the interception data set (Figure 11). While the inclusion of a stratified model approach did improve the model at larger scales, it seems likely that the inclusion of parameters which describe large-scale features such as canopy gaps (total open area) are sufficient alone to reduce the potential of systematic bias when upscaling from a point to larger grid sizes. However, this needs to be further tested on scales larger than 62,500 m^2 (the maximum allowable domain size within this study).

The distribution of storm based events within this data set showed an underlying sigmoidal shaped distribution similar to prior interception studies [*Satterlund and Haupt*, 1967; *Schmidt and Gluns*, 1991]. Akin to those studies, this data showed an initial efficiency increase until I_{max} was reached at which point the efficiency demonstrated a clear falling limb.

This model was compared to the most used snow interception model to date [*Essery et al*., 2009; *Hedstrom and Pomeroy*, 1998] and showed an r^2 increase of 25% for the point scale as well as a reduction in the RMSE by 53%. At all grid scales, the *Hedstrom and Pomeroy* model showed an RMSE increase of 75–114% when compared to the Moeser et al. model. The Moeser et al. model showed a minor underestimate of all estimated interception values. However, when compared to the *Hedstrom and Pomeroy* model, this underestimate is reduced by ~40%. The principle deficiency leading to the substantial interception underestimates within the *Hedstrom and Pomeroy* model was due to the underlying exponential decay interception efficiency distribution. These underestimates were further offset from the use of an I_{max} equation (equation (3)) which integrated unique tree species specific multipliers from a study which derived them from the branch scale. As *Schmidt and Gluns* [1991] notes, extrapolating results from branch interception to that of a tree would exhibit efficiency and interception values greater than that for a single branch due to the increased probability of lower canopy structures collecting particle bounce.

The paired correspondence and k-means cluster analysis showed higher correlations of I_{max} to the novel canopy descriptors than LAI and canopy closure. Mean distance to canopy yielded the highest correlations to I_{max} (R: 0.83) and was the most significant variable within the model. This variable also increased model performance at low interception efficiency ranges and helps when using a gridded modeling approach in terrain with heterogeneous to light canopy. Total open area (R: 0.76) also showed high correlations to I_{max} and no cross correlation issues with mean distance to canopy or canopy closure. The I_{max} integrated within the *Hedstrom and Pomeroy* model utilized fresh snow density and LAI. However, the initial correlation analysis showed reduced correlation of I_{max} to LAI (R: 0.58) as compared to canopy closure (R: 0.76). Correlations of fresh snow density were also minimal implying that at least when storm based I_{max} is estimated, (1) the overhead canopy elements play a larger part than the density of the falling snow and (2) the use canopy closure give more robust estimations than LAI. The analysis also showed a high degree of cross correlation between canopy closure, LAI and mean tree height negating the utility of a pairing of CC and LAI in one model.

The independent parameters from this model are easily derived pending the existence of aerial LiDAR data and the vector searching algorithm scripts used within this study can be easily transferred to other data sets. All scripts related to this algorithm are freely available upon request.

Acknowledgments

This project was funded by the Swiss National Science Foundation (SNF; project 200021_146184/1). Field help was given by Clare Webster, Nena Griessinger, Saskia Gindraux, Franziska Zieger, Franziska Zahner, Jiri Roubinek, and Mathias Rieckh of the WSL Institute for Snow and Avalanche Research SLF, snow hydrology group. Programming support was given by Jan Magnusson and Florian Kobierska also of the snow hydrology group. Aerial LiDAR data support was given by Felix Morsdorf of the Remote Sensing Laboratories within the Department of Geography at the University of Zurich. All data used within this study are available upon request from the corresponding author (moeser@slf.ch).

References

Breda, N. (2003), Ground-based measurements of leaf area index: A review of methods, instruments and current controversies, *J. Exp. Bot.*, *54*(392), 2403–2417.

Brundl, M., P. Bartelt, M. Schneebeli, and H. Fluhler (1999), Measuring branch defection of spruce branches caused by intercepted snow load, *Hydrol. Processes*, *13*(14–15), 2357–2369.

Bunnell, F. L., R. S. McNay, and C. C. Shank (1985), Trees and snow: the deposition of snow on the ground—A review and quantitative synthesis, *IWIFR-17*, Minist. of Environ. and For., Vic. Electr. Coop., Victoria, Tex.
Calder, I. R. (1991), *Evaporation in the Uplands*, John Wiley, Chichester, U. K.
Car, J. (2002), *Data Visualization in the Geological Sciences*, Prentice Hall, Upper Saddle River, N. J.
Carpenter, L. G. (1901), Forests and snow, *Bull. 55*, Colo. Agric. Exp. Stn. of the Agric. Coll. of Colo., Fort Collins.
Chang, M. (2003), *Forest Hydrology: An Introduction to Water and Forests*, 392 pp., CRC Press, Boca Raton, Fla.
Church, J. E. (1912), The conservation of snow: Its dependence on forests and mountains, *Sci. Am. Suppl.*, *74*, 152–155.
Essery, R., N. Rutter, J. Pomeroy, R. Baxter, M. Stahli, D. Gustafsson, A. Barr, P. Bartlett, and K. Elder (2009), SNOWMIP2: An evaluation of forest snow process simulations, *Bull. Am. Meteorol. Soc.*, *90*(8), 1120–1135.
Golding, D. L., and R. H. Swanson (1986), Snow distribution in clearings and adjacent forest, *Water Resour. Res.*, *22*(13), 1931–1940.
Greenacre, M., and J. Blasius (1994), *Correspondence Analysis in the Social Sciences*, 370 pp., Academic, Waltham, Mass.
Guntner, A., J. Stuck, S. Werth, P. Doll, K. Verzano, and B. Merz (2007), A global analysis of temporal and spatial variations in continental water storage, *Water Resour. Res.*, *43*, W05416, doi:10.1029/2006WR005247.
Hedstrom, N. R., and J. W. Pomeroy (1998), Measurements and modelling of snow interception in the boreal forest, *Hydrol. Processes*, *12*(10–11), 1611–1625.
Hyer, E. J., and S. J. Goetz (2004), Comparison and sensitivity analysis of instruments and radiometric methods for LAI estimation: Assessments from a boreal forest site, *Agric. For. Meteorol.*, *122*(3–4), 157–174.
Kobayashi, D. (1987), Snow accumulation on a narrow board, *Cold Reg. Sci. Technol.*, *13*, 239–245.
Lorenzo-Seva, U., M. Van de Velden, and H. Kiers (2009), Oblique rotation in corrrespondence analysis: A step forward in search of the simplest interpretation, *Br. J. Math. Stat. Psychol.*, *62*, 583–600.
Lovell, J. L., D. L. B. Jupp, D. S. Culvenor, and N. C. Coops (2003), Using airborne and ground-based ranging lidar to measure canopy structure in Australian forests, *Can. J. Remote Sens.*, *29*(5), 15.
Lundberg, A., and S. Halldin (2001), Snow interception evaporation-rates, processes and measurement techniques, *Theor. Appl. Climatol.*, *70*, 117–133.
Lundberg, A., I. Calder, and R. Harding (1998), Evaporation of intercepted snow: Measurement and modelling, *J. Hydrol.*, *206*(3–4), 151–163.
Miller, D. H. (1964), *Interception Processes During Snowstorms*, U.S. Dep. of Agric., Berkeley, Calif.
Moeser, D., J. Roubinek, P. Schleppi, F. Morsdorf, and T. Jonas (2014), Canopy closure, LAI and radiation transfer from airborne LiDAR synthetic images, *Agric. For. Meteorol.*, *197*, 158–168.
Moeser, D., F. Morsdorf, and T. Jonas (2015), Novel forest structure metrics from airborne LiDAR data for improved snow interception estimation, *Agric. For. Meteorol.*, *208*, 40–49.
Montesi, J., K. Elder, R. A. Schmidt, and R. E. Davis (2003), Sublimation of intercepted snow within a subalpine forest canopy at two elevations, *J. Hydrometeorol.*, *5*(5), 763–773.
Morsdorf, F., et al. (2004), LIDAR-based geometric reconstruction of boreal type forest stands at single tree level for forest and wildland fire management, *Remote Sens. Environ.*, *92*(3), 353–362.
Morsdorf, F., B. Kötz, E. Meier, K. I. Itten, and B. Allgöwer (2006), Estimation of LAI and fractional cover from small footprint airborne laser scanning data based on gap fraction, *Remote Sens. Environ.*, *104*(1), 50–61.
Nakai, Y., H. Kitahara, and T. Saito (1994), Snow interception by forest canopies: Weighing a conifer tree, meteorological observation and analysis by the Penman-Montheith formula, in *Snow and Ice Covers: Interactions with the Atmosphere and Ecosystems (Proceedings of Yokohama Symposia J2 and J5)*, IAHS Publ. 223, pp. 227–236, IAHS Press, Wallingford, U. K.
Nakai, Y., T. Sakamoto, T. Terajima, K. Kitamura, and T. Shirai (1999), The effect of canopy-snow on the energy balance above a coniferous forest, *Hydrol. Processes*, *113*, 2371–2382.
Pfister, R., and M. Schneebeli (1999), Snow accumulation on boards of different sizes and shapes, *Hydrol. Processes*, *13*(14–15), 2345–2355.
Pomeroy, J., D. M. Gray, K. Shook, B. Toth, R. Essery, A. Pietroniro, and N. R. Hedstrom (1998a), An evaluation of snow accumulation and ablation processes for land surface modeling, *Hydrol. Processes*, *12*, 2339–2367.
Pomeroy, J. W., J. Parviainen, N. Hedstrom, and D. M. Gray (1998b), Coupled modelling of forest snow interception and sublimation, *Hydrol. Processes*, *12*, 2317–2337, doi:10.1002/(SICI)1099-1085(199812)12:15<2317::AID-HYP799>3.0.CO;2-X.
Riaño, D., F. Valladares, S. Condés, and E. Chuvieco (2004), Estimation of leaf area index and covered ground from airborne laser scanner (Lidar) in two contrasting forests, *Agric. For. Meteorol.*, *124*(3–4), 269–275.
Rutter, N., R. Essery, J. Pomeroy, N. Altimir, K. Andreadis, I. Baker, A. Barr, and P. Bartlett (2009), Evaluation of forest snow processes models (SnowMIP2), *J. Geophys. Res.*, *114*, D06111, doi:10.1029/2008JD011063.
Satterlund, D. R., and H. F. Haupt (1967), Snow catch by conifer crowns, *Water Resour. Res.*, *3*(4), 1035–1039, doi:10.1029/WR003i004p01035.
Schleppi, P., M. Conedera, I. Sedivy, and A. Thimonier (2007), Correcting non-linearity and slope effects in the estimation of the leaf area index of forests from hemispherical photographs, *Agric. For. Meteorol.*, *144*(3–4), 236–242.
Schmidt, R. A., and D. R. Gluns (1991), Snowfall interception on branches of three conifer species, *Can. J. For. Res.*, *21*(8), 1262–1269.
Seber, G. A. F. (1984), Multivariate distributions, in *Multivariate Observations*, pp. 17–58, John Wiley, Hoboken, N. J.
Solberg, S. (2010), Mapping gap fraction, LAI and defoliation using various ALS penetration variables, *Int. J. Remote Sens.*, *31*(5), 1227–1244.
Solberg, S., A. Brunner, K. Hanssen, H. Lange, E. Naesset, M. Rautiainen, and P. Stenberg (2009), Mapping LAI in a Norway spruce forest using airborne laser scanning, *Remote Sens. Environ.*, *113*(11), 2317–2327.
Späth, H. (1986), Cluster dissection and analysis: theory, FORTRAN programs, examples, (Translator: Johannes Goldschmidt.) Ellis Horwood Ltd Wiley, Chichester 1985, 226 pp., Biometrical J., *28*, 182, doi:10.1002/bimj.4710280207.
Storck, P., D. P. Lettenmaier, and S. M. Bolton (2002), Measurement of snow interception and canopy effects on snow accumulation and melt in a mountainous maritime climate, Oregon, United States, *Water Resour. Res.*, *38*(11), 1223, doi:10.1029/2002WR001281.
Suzuki, K., and Y. Nakai (2008), Canopy snow influence on water and energy balances in a coniferous forest plantation in northern Japan, *J. Hydrol.*, *352*(1–2), 126–138.
Taylor, K. E. (2001), Summarizing multiple aspects of model performance in a single diagram, *J. Geophys. Res.*, *106*(D7), 7183.
Tennyson, L. C., P. F. Ffolliott, and D. B. Thorud (1974), Use of time-lapse photography to assess potential interception in arizona ponderosa pine, *Water Resour. Bull.*, *10*, 1246–1254, doi:10.1111/j.1752-1688.1974.tb00641.x.
Thimonier, A., I. Sedivy, and P. Schleppi (2010), Estimating leaf area index in different types of mature forest stands in Switzerland: A comparison of methods, *Eur. J. For. Res.*, *129*(4), 543–562.
Troendle, C. A., and J. R. Meiman (1986), The effect of patch clear-cutting on the water balance of a subalpine forest slope, paper presented at Phoenix Symposium on 54th Western Snow Conference, Phoenix, Ariz.
US Army Corps of Engineers (1956), *Snow Hydrology: Summary Report of the Snow Investigations*, 437 pp., North Pac. Div., Portland, Oreg.

van de Velden, M., and H. A. L. Kiers (2005), Rotation in correspondence analysis, *J. Classif.*, *22*(2), 251–271.
Varhola, A., et al. (2010a), The influence of ground- and lidar-derived forest structure metrics on snow accumulation and ablation in disturbed forests, *Can. J. For. Res.*, *40*(4), 812–821.
Varhola, A., N. C. Coops, M. Weiler, and R. D. Moore (2010b), Forest canopy effects on snow accumulation and ablation: An integrative review of empirical results, *J. Hydrol.*, *392*(3–4), 219–233.
Veatch, W., P. D. Brooks, J. R. Gustafson, and N. P. Molotch (2009), Quantifying the effects of forest canopy cover on net snow accumulation at a continental, mid-latitude site, *Ecohydrology*, *2*(2), 115–128.
Winkler, R. D., D. L. Spittlehouse, and D. L. Golding (2005), Measured differences in snow accumulation and melt among clearcut, juvenile, and mature forests in southern British Columbia, *Hydrol. Processes*, *19*(1), 51–62.
Zhao, K., S. Popescu, X. Meng, Y. Pang, and M. Agca (2011), Characterizing forest canopy structure with lidar composite metrics and machine learning, *Remote Sens. Environ.*, *115*(8), 1978–1996.